Materials Science and Engineering, 31 (1977) 141 - 152
© Elsevier Sequoia S.A., Lausanne — Printed in the Netherlands

Lattice Vibrations in Graphite and Intercalation Compounds of Graphite*

M. S. DRESSELHAUS**,†, G. DRESSELHAUS***, P. C. EKLUND**,† and D. D. L. CHUNG†,††
Massachusetts Institute of Technology Cambridge, MA 02139 (U.S.A.)

SUMMARY

The lattice modes of pure graphite can be divided into intraplanar displacements and interplanar displacements. Upon intercalation, the intraplanar vibration frequencies are only slightly shifted, though their Raman and infrared intensities can be greatly changed. These characteristics of the intraplanar vibrational modes are interpreted in terms of symmetry changes associated with intercalation. These symmetry changes give rise to both in-plane and *c*-axis zone folding effects. Detailed results are reported for the Raman spectra of graphite–halogen acceptor compounds and graphite–alkali metal donor compounds. In the case of the graphite–halogen compounds, spectra showing both graphitic modes and intercalate modes are interpreted in terms of this symmetry model. In the case of the alkali metal compounds, the spectra for stage 1 compounds are considered separately from those for higher stage compounds. Particular attention is given both to the broad asymmetric Breit–Wigner high frequency structure and to the sharp doublet structure observed at intermediate frequencies. Infrared spectra of lattice modes in graphite intercalation compounds are reported.

The lattice dynamics of pristine graphite have been studied by a variety of techniques such as inelastic neutron scattering, Raman scattering, and infrared spectroscopy. In this paper the observed lattice modes in the intercalation compounds are related either to the modes in pristine graphite or to the modes in the intercalate layers. In the present analysis, the modes in the intercalation compounds are treated as a perturbation to the symmetry of pristine graphite. The characteristic features of the observed spectra can be classified in terms of (1) graphite modes for compounds with stages $n > 2$, (2) graphite modes for stage 1 and 2 compounds, and (3) intercalate modes. The presentation given here follows this organization. In the case of stage 1 alkali metal compounds, in-plane and *c*-axis zone folding effects are important and are treated explicitly. Emphasis is given to Raman spectra observed for graphite–halogen and graphite–alkali metal compounds. These spectra are interpreted in terms of a variety of symmetry considerations relevant to the basic symmetry of pristine graphite.

Pristine graphite, which crystallizes according to the D_{6h}^4 space group, has twelve vibrational modes, consisting of three acoustic modes ($A_{2u} + E_{1u}$), three infrared-active modes ($A_{2u} + E_{1u}$), four Raman-active modes ($2E_{2g}$) and two silent modes ($2B_{1g}$) (see Fig. 1). These lattice modes in pristine graphite have been studied by Raman scattering [1 - 3], infrared spectroscopy [1, 2, 4 - 6] and inelastic neutron scattering [7].

The frequencies of the in-plane Raman-active E_{2g_2} mode and the infrared-active E_{1u} mode are well established at $1\,582 \pm 1$ cm^{-1} [1, 2] and at $1\,588 \pm 2$ cm^{-1} [2, 6], respectively. Because of the strong intralayer force constants relative to the interlayer force constants, the vibrational frequencies of these modes are nearly the same, and are almost

*Work supported by the United States ONR Grant #N00014-77-C-0053.
**Department of Electrical Engineering and Computer Science and Center for Materials Science and Engineering.
***Francis Bitter National Magnet Laboratory, supported by the United States National Science Foundation.
†Visiting Scientist, Francis Bitter National Magnet Laboratory.
††Department of Materials Science and Engineering and Center for Materials Science and Engineering.

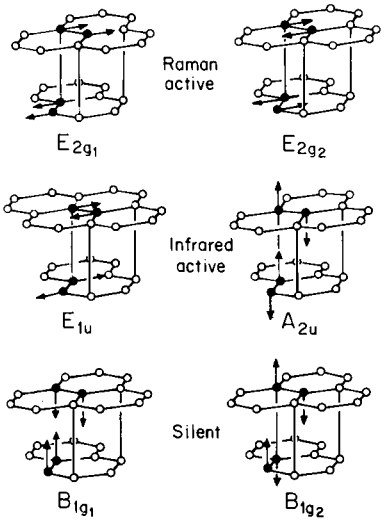

Fig. 1. Γ-point optical mode displacements and symmetries for the graphite lattice.

entirely determined by the simple optical displacements of the two inequivalent carbon atoms in a single layer plane. The small frequency difference of ~6 cm^{-1} between the Raman-active E_{2g_2} mode and the infrared-active E_{1u} mode, is associated with interlayer force constants because of the differences of these modes with respect to interplanar displacements (see Fig. 1). This small frequency difference thus provides a measure of the magnitude of these interlayer force constants.

The out-of-plane infrared active A_{2u} mode has recently been reported at 868 ± 1 cm^{-1} [6]. The identification of the low frequency Raman-active E_{2g_2} mode at 48 cm^{-1} and the silent out-of-plane B_{1g} mode at 128 cm^{-1} has been made on the basis of inelastic neutron scattering measurements on the low frequency (<470 cm^{-1}) phonon branches [7].

The identification of the E_{2g_1} mode is significant in establishing the magnitude of the interlayer force constants. In the graphite lattice (see Fig. 1), we note that there are two inequivalent planar sites: A sites (carbon atoms having the same (x, y) coordinates as a function of z) and B sites (carbon atoms having different (x, y) coordinates on alternate layer planes). In the E_{2g} modes, the A atoms on adjacent layers have out-of-phase displacements with respect to each other as do the B atoms, while for the E_{1u} mode and the pure translational zero frequency mode, the A atom displacements on adjacent planes are in-phase, as are the B atom displacements. Since the interlayer coupling results in a perturbation whereby the *acoustic* E_{2g_1} mode, with out-of-phase displacements on adjacent planes, is up-shifted in frequency relative to the pure translational mode at $\omega = 0$ with in-phase displacements, this interaction must correspondingly downshift the E_{2g_2} out-of-phase optical mode relative to the E_{1u} in-plane optical mode. The resulting splittings in the acoustic and optical modes are approximately related by $\omega^2(E_{2g_1}) \approx \omega^2(E_{1u}) - \omega^2(E_{2g_2})$. While this argument does not quantitatively account for the frequency splitting of the E_{1u} and E_{2g_2} modes it does account for the relative ordering of the E_{1u} and E_{2g_2} modes. Since $\omega^2(E_{2g_1})$ is only 2.3×10^3 cm^{-2}, the splitting predicted for the optical E_{1u} and E_{2g_2} modes is <1 cm^{-1}. Because this predicted splitting is so small, other physical mechanisms would be expected to make contributions of similar magnitudes [8].

Analysis of the inelastic neutron scattering data [7] has provided phonon dispersion curves for the two lowest frequency phonon branches along ΓM (see the hexagonal Brillouin zone in Fig. 2). Near the M-point, the two lowest frequency modes are nearly

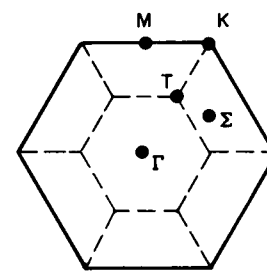

Fig. 2. The in-plane Brillouin zone cross-section (k_z = 0) for pristine graphite (solid line). The dashed lines show the extended zone scheme appropriate to the C_8X structure.

degenerate at ~466 cm^{-1} and these modes correspond to z-axis displacements [7]. In the analysis of the neutron scattering data, a Born–von Karman model was used [7] to fit the measured phonon branches and this model provided phonon dispersion relations throughout the Brillouin zone as shown in Fig. 3. Because these inelastic neutron scattering measurements were limited to frequencies <470 cm^{-1}, these dispersion relations can only be regarded as qualitative in

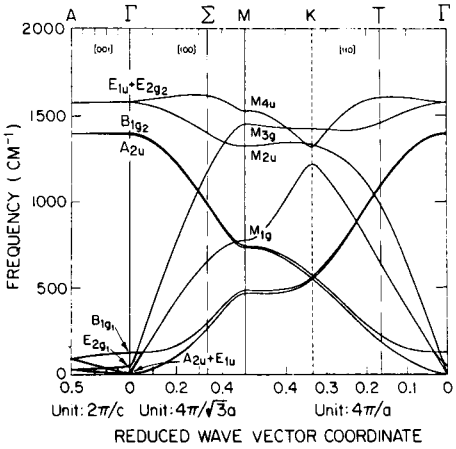

Fig. 3. Full-zone graphite phonon dispersion curves from ref. 7. The Γ-point symmetries for the graphite structure are indicated. At the *M*-point the indicated symmetries are those for the in-plane vibrations of a single layer.

the region of the optic modes. In this connection we note the discrepancy between these dispersion relations and the recent direct measurement of the zone center A_{2u} phonon frequency at 868 cm^{-1} [6].

Nevertheless, many of the features of these dispersion relations are qualitatively correct and offer a guide for the interpretation of lattice mode spectra in both graphite and intercalation compounds based on graphite.

Since the graphitic layer structure is preserved upon intercalation, the mode structure for the carbon atom vibrations in the intercalation compounds can be related to the modes in pristine graphite [9]. Justification for this approach comes from the observation that for the in-plane modes the interplanar force constants, which would be expected to be most sensitive to intercalation, play a minor role in determining the in-plane vibrational frequencies. This hypothesis is supported by experimental observations of in-plane carbon atom modes in graphite intercalation compounds at frequencies close to those corresponding to pristine graphite.

Based on these ideas, a model for the in-plane mode structure for graphite intercalation compounds has recently been developed [9], and specific applications have been made to a variety of symmetry arrangements of the intercalate species relative to the graphitic layers (*e.g.*, C_6X, C_8X, $C_{18}X_2$, $C_{24}X_2$). We will consider here the simple case of C_8X, corresponding to the stage 1 alkali metal compounds.

The ordering of the intercalate species in the intercalate layer plane relative to the graphitic plane for C_8X is shown in Fig. 4.

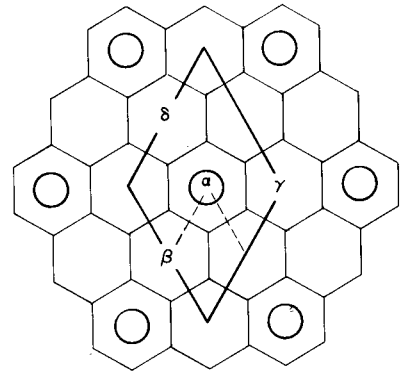

Fig. 4. Position of the intercalate species X (open circles) relative to the graphite layer (hexagonal net) for the C_8X structure. The solid lines indicate the unit cell for C_8X while the dashed lines indicate the C_2 unit cell. The 4 equivalent sites for the intercalation species within each unit cell are indicated by α, β, γ, δ.

Since adjacent carbon atoms in a layer plane of pristine graphite are inequivalent, a layer plane unit cell contains two carbon atoms, as shown in Fig. 4 (dashed lines). However, for the stage 1 alkali metal intercalation compounds a graphitic layer plane unit cell contains 8 carbon atoms, as shown in Fig. 4 (solid lines). (We note that for C_8X each intercalate site is crystallographically equivalent.) Thus, the real space unit cell corresponding to the C_8X structure in Fig. 4 is 4 times as large as that for pristine graphite and, correspondingly, the C_8X planar unit cell in reciprocal space will be 1/4 as large.

This relation between the unit cells in reciprocal space suggests that the modes for the intercalation compounds can be related to those for pristine graphite by a "folding" of the Brillouin zone for pristine graphite onto that for the intercalate compounds. The zone folding procedure must, however, be considered in 3 dimensions because different effects are associated with *c*-axis folding as compared with in-plane folding.

The larger unit cell in the *c*-direction arises both from the presence of stages in the intercalation compounds and from the different possible locations of the intercalate species

relative to the carbon atoms. For example, in Fig. 4, there are 4 equivalent choices for locating the intercalate atom X in the C_8X structure (*e.g.*, the unit cell of Fig. 4 has four equivalent sites labeled $\alpha, \beta, \gamma, \delta$). Intercalate layer planes corresponding to each choice of α, β, γ or δ occur with equal probability in C_8K; here, the layer planes are ordered in some sequence such as α, β, γ and δ, so that the real space unit cell for a first stage C_8K compound contains 4 graphitic layers. Whether or not all equivalent sites are equally occupied or interplanar site ordering occurs, some general statements can be made about *c*-axis zone folding. In each layer plane, the in-plane area of the Brillouin zone for C_8X would be 1/4 as large as is indicated by the inner dashed hexagon in Fig. 2. Since the phonon dispersion curves along k_z in Fig. 3 show small dispersion for the acoustic branches and almost no dispersion along the optic branches, one would expect the k_z zone folding to give rise to the following two effects. Firstly, the new modes arising from the mapping of the larger zone onto the smaller zone, will occur at almost the same frequency as the pure graphitic modes, thereby giving rise to a "one dimensional density of states" type broadening of the Raman and infrared lines. The density of states aspect of the folded zone-center modes is further reinforced if the interlayer site ordering is imperfect, resulting in a distribution in the size of the *c*-axis unit cells. The second zone-folding effect is to increase the number of observable contributions to the infrared and Raman spectra from otherwise symmetry-forbidden modes. Since the phonons away from $\vec{k} = 0$ in pristine graphite have lower symmetry than the $\vec{k} = 0$ phonons, these new modes arising from zone folding effects would normally be both infrared and Raman active, thereby contributing both to observed infrared and Raman spectra in the intercalation compounds.

By contrast to the small k_z-axis dispersion, a large in-plane dispersion occurs for directions in the k_x, k_y plane. Since the in-plane forces are much stronger than the interplanar forces, there is a higher degree of local in-plane site ordering than interplanar site ordering. Thus, in-plane folding is expected to give rise to frequencies in the infrared and Raman spectra which do not correspond to $\vec{k} = 0$ phonons in pristine graphite. The particular frequencies at which the new modes occur will depend on the in-plane unit cell, because for each type of unit cell, different $\vec{k}$-point modes are folded onto $\vec{k} = 0$ for pristine graphite. A listing of the $\vec{k}$-points for the pristine graphite zone which are folded back onto $\vec{k} = 0$ for the intercalation compounds is given in Table 1 for real space

TABLE 1

In-plane folding of graphite Brillouin Zone onto the zone for the intercalation compounds

Chemical formula for in-plane unit cell	High symmetry points which fold onto $\vec{k} = 0$ for C_2
C_2	Γ
C_6X	Γ, K
C_8X	Γ, M
$C_{18}X_2$	Γ, K, Σ
$C_{24}X_2$	Γ, K, M, T

unit cells containing 6, 8, 18 and 24 in-plane carbon atoms. The entries for C_6X and C_8X correspond to the stage 1 alkali metal compounds, while $C_{9n}X$ and $C_{12n}X$ have been proposed for stages $n \geqslant 2$ [10]. Of particular significance to the present discussion, is the mapping of point M in pristine graphite into $\vec{k} = 0$ for the stage 1 alkali metal C_8X compounds.

The advantage of superimposing the high symmetry of pristine graphite (D_{6h}) as an approximate symmetry in the lower symmetry intercalation compounds (D_2) can be appreciated by the following consideration. In pristine graphite there are 4 atoms/unit cell giving rise to $4 \times 3 - 3 = 9$ optic branches with 6 distinct $\vec{k} = 0$ frequencies. In the case of the simple intercalation compound C_8X with $\alpha, \beta, \gamma, \delta$ planar stacking there are 36 atoms per unit cell, resulting in $36 \times 3 - 3 = 105$ optic modes. All of these modes will have distinct frequencies because the four irreducible representations, $\Gamma_1, \Gamma_2, \Gamma_3$ and Γ_4 of D_2 are 1-dimensional. Almost all of these modes will contribute to the observed spectra since all modes are Raman-active, and except for Γ_1, all modes are also infrared-active. The concept of approximate D_{6h} symmetry permits us to make statements about the relative intensity of Raman-active modes in the intercalation compounds and about the grouping of their normal mode frequencies.

Since the in-plane interactions are much stronger than the interplanar interactions, an approximate treatment of the lattice modes in the intercalation compounds can be effected by considering only the in-plane unit cell (see Fig. 4). With 8 carbon atoms in a planar unit cell there will be 16 in-plane modes and 8 out-of-plane modes. Classifying their symmetries according to the irreducible representations of D_{6h} gives the symmetries A_{1g}, A_{2g}, B_{1u}, B_{2u}, $3E_{1u}$ and $3E_{2g}$ for the in-plane modes, and the symmetries $2A_{2u}$, $2B_{1g}$, E_{1u} and E_{2g} for the out-of-plane modes [9]. One of the E_{2g} modes in the C_8X intercalation compound $E_{2g}(E_{2g_2})$ corresponds directly to the E_{2g_2} mode of pristine graphite (indicated in parentheses) and is shown in Fig. 5(a); this mode in the intercalation compound will thus lie close to the E_{2g_2} graphite mode frequency. A second Raman-active mode in the intercalation compound is expected at a somewhat lower frequency and is associated with a folding back of the M_{3g} mode to the zone center. Since there are 3 equivalent M points in the Brillouin zone, the mapping of the 3 non-degenerate M_{3g} graphite modes onto the Γ-point of the smaller zone results in a 3-fold multiplet structure having E_{2g} and A_{2g} symmetries, the E_{2g} mode being Raman-active and the A_{2g} mode being silent. The normal mode displacements for this $E_{2g}(M_{3g})$ mode are shown in Fig. 5(b). Raman-active lines also arise from a folding of the M_{1g} mode onto the Γ-point. In this case, the M_{1g} non-degenerate modes coming from the 3 equivalent M-points give rise to zone center modes with $E_{2g} + A_{1g}$ symmetries, both of which are Raman-active and have the mode patterns shown in Fig. 5(c) and (d). In all the modes shown in Fig. 5, there is no displacement for the intercalate atom (large circle). In Fig. 5(b) and (d), the carbon atom displacements designated by ω and ω^2 indicate that these displacements are, respectively, $2\pi/3$ and $4\pi/3$ out-of-phase relative to the displacements denoted by 1. The partners for these modes are generated by interchanging ω and ω^2.

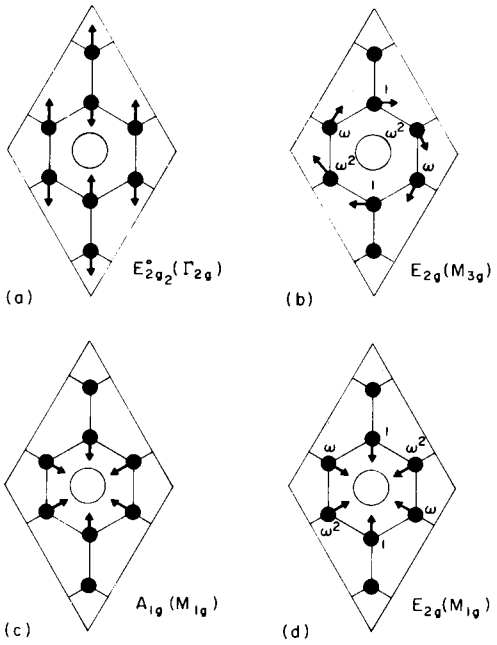

Fig. 5. The in-plane Raman active modes for the C_8X unit cell having D_{6h} symmetry. The symmetry label in parentheses is that appropriate to the mode in the absence of the intercalate. The two-fold degenerate, E_{2g}, modes originating from the M_{3g} and M_{1g} zone edge modes have atomic displacements related by phase factors 1, ω, ω^2 ($\omega = e^{2\pi i/3}$). The degenerate partner is the complex conjugate or orthogonal displacement of the mode shown in the Figure. All of the E_{2g} modes become coupled through lattice distortions introduced by the presence of the intercalate species. The intercalate, X, is shown as a large open circle with no displacement.

A similar analysis can be made to yield the mode patterns for the in-plane infrared-active modes. For a single graphitic layer there is no infrared-active optical E_{1u} mode, since the 1 588 cm^{-1} mode in pristine graphite results from the AB planar stacking. Although C_8X has no $E_{1u}(E_{1u})$ mode, higher stage compounds can have such an infrared-active optical mode. Returning to the C_8 in-plane unit cell, zone folding from the 3 equivalent M-point M_{4u} and M_{2u} modes gives rise to modes with ($E_{1u} + B_{1u}$) and ($E_{1u} + B_{2u}$) symmetries, respectively, with only the E_{1u} modes being infrared-active. Because of the placement in frequency of the M-point in-plane optical modes in Fig. 3, the $E_{1u}(M_{4u})$ and the $E_{1u}(M_{2u})$ modes arising from zone-folding effects are expected to be high-frequency modes, and the mode patterns for these modes are shown in Fig. 6(a) and (b), respectively. A third E_{1u} mode at $\omega = 0$ corresponding to pure translations is also present but does not give rise to infrared activity. These infrared-active modes can also become Raman-active if the larger c-axis unit cell is considered so that inversion symmetry is no longer applicable. The polarizability tensors for the $E_{1u}(M_{4u})$ and $E_{1u}(M_{2u})$ modes may be larger than that for the E_{1u} mode in pristine

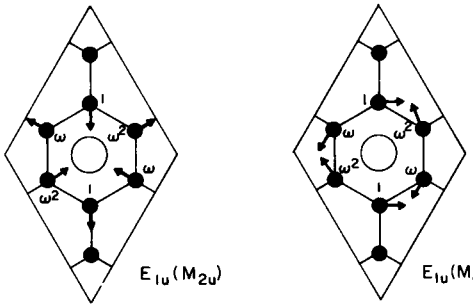

Fig. 6. The in-plane infrared active modes for the C_8X unit cell. The phase factors and notations are the same as for Fig. 5.

graphite; thus, these new E_{1u} modes are expected to have relatively high Raman intensities. Coupling between all modes with the same symmetry in a partially disordered D_2 structure can give rise to a broad, asymmetric line within which the individual modes are unresolved. For compounds with stage $n \geqslant 2$, the real space unit cell is large and not known in detail [11, 12], and thus it is not yet possible to carry out a quantitative analysis of zone folding effects for these compounds.

Almost all of the Raman scattering experiments on graphite intercalation compounds have been performed on *c*-faces using a Brewster angle back-scattering geometry. Incident radiation at 4 880 Å and 5 145 Å is conveniently provided by a cw argon-ion laser. The scattered radiation is collected at 90 ° to the sample surface and is analyzed by a double grating monochromator. Almost all materials studied to date exhibit Raman lines similar to those shown in Fig. 7 for lamellar compounds of graphite intercalated with the halogens Br_2, IBr, ICl, and the alkali metal Rb (stage 3 $C_{36}Rb$) [13 - 15]. The single E_{2g_2} peak of pure graphite is replaced in the intercalation compounds by a doublet, having a separation of ~ 20 cm^{-1}, with the lower frequency peak near the pure E_{2g_2} graphite line. In the case of the halogen compounds, the frequencies of both peaks increase slightly with increasing intercalate concentration, but the frequency difference between the two peaks is essentially independent of intercalate concentration [13]. For example, in graphite–Br_2 lamellar compounds, the frequency of each of the doublet components increases by ~ 7 cm^{-1} from a 0.9 mole% (stage 14) Br_2 compound to a 5.6 mole% ($\sim$ stage 2) Br_2 compound. Similar structures have also been

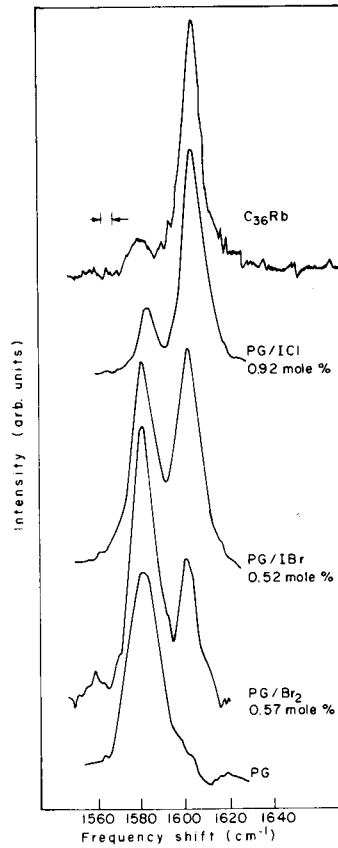

Fig. 7. Experimental Raman scattering spectra for several intercalated graphite compounds. The position of each peak in the doublet structure is nearly independent of intercalate species and concentration. The resolution is indicated by the arrows.

reported in graphite–HNO_3 [13] and in graphite–$AlCl_3$, graphite–SbF_5 and $C_{36}Cs$ [14]. A slight dependence of the frequencies of the doublet components on the intercalate species has been reported [13, 14]. Because this dependence on intercalate concentration is small, both lines are identified with carbon atom vibrations. On the other hand, there is a strong dependence of the relative intensities of the doublet components on intercalate concentration. Increasing the intercalate concentration causes the intensity of the lower frequency component to decrease and the intensity of the upper frequency component to increase.

An identification of the lower frequency component is made with the E_{2g_2} carbon atom vibrations in graphite layer planes which are surrounded by other graphite planes and is denoted by $E^{\circ}_{2g_2}$. This identification is supported by the proximity of this mode to the E_{2g_2} mode of pristine graphite, by the low

intensity of the $E^{\circ}_{2g_2}$ line in the low stage halogen compounds, and by the vanishing of the $E^{\circ}_{2g_2}$ line in the stage 2 and stage 1 alkali metal intercalation compounds.

The upper frequency component in these spectra is identified with an E_{2g} (E_{2g_2})-type graphite-mode but occurring in a carbon plane adjacent to an intercalate layer plane. (This mode labeled E'_{2g_2} mode would correspond in a C_8X planar structure to the E_{2g} (E_{2g_2}) mode shown in Fig. 5(a).) Support for this identification comes from the absence of the E'_{2g_2} line in pristine graphite and the increase of its intensity with increasing intercalate concentration. The occurrence of E'_{2g_2} at a higher frequency than $E^{\circ}_{2g_2}$ arises from the perturbation of the in-plane force constants and from the distortion of certain in-plane carbon site positions by the nearby intercalate species, thereby resulting in a lowering of symmetry for the graphite in-plane structure. This lowering of symmetry increases the size of the real space unit cell, decreases the size of the reciprocal space unit cell, and causes various modes for pristine graphite to map into the zone center for the smaller Brillouin zone. Since a number of the zone-folded modes also have E_{2g} symmetry, they will interact with the $E_{2g}(E_{2g_2})$ mode. Furthermore, because the zone-folded E_{2g} modes lie lower in frequency than the $E_{2g}(E_{2g_2})$ mode (see Fig. 3) this interaction will upshift the $E_{2g}(E_{2g_2})$ mode to frequencies higher than the occurrence of E_{2g_2} in pristine graphite. The strength of the perturbation introduced by the adjacent intercalate species on the in-plane carbon-atom force constants determines the magnitude of this upshift in frequency. The small magnitude of this frequency upshift indicates that the perturbation due to the presence of adjacent intercalate species is generally weak. The model presented here suggests that the perturbation will be stronger for intercalate molecules tipped out of the intercalate layer plane than for molecules lying in the plane. This interpretation further predicts that the E'_{2g_2} mode will be upshifted with respect to $E^{\circ}_{2g_2}$ for both acceptor and donor compounds, since the mechanism giving rise to the frequency shift is based primarily on a lowering of symmetry due to the presence of a nearby intercalate layer. The results in Fig. 7 and Table 2 show the E'_{2g_2} mode to be upshifted with respect to $E^{\circ}_{2g_2}$ for both acceptor (halogen) and donor (alkali metal) intercalation compounds.

When the $E^{\circ}_{2g_2}$ mode at 1 582 cm^{-1} is observed in the various intercalation compounds (see Table 2), it is almost unshifted from its position in pristine graphite. On the other hand, the intensity of this line varies by an order of magnitude for the various compounds cited in this Table. Correspondingly, the frequency of the E'_{2g_2} lines in Table 2 is essentially independent of intercalate species and increases slightly with increasing intercalate concentration, although large variations in the intensity of this line occur for the variety of examples cited in this Table.

Using simple geometric considerations we can distinguish three kinds of carbon atom sites, depending on whether the carbon atom: (1) does not lie in a layer plane adjacent to an intercalate layer plane, (2) does lie in a plane adjacent to an intercalate layer plane but is not a nearest neighbor to an intercalate site, or (3), is a nearest neighbor to an intercalate site. For a stage n compound the fraction of C atoms not bordering intercalate planes is $f_0 = 1 - (2/n)$, $n \leqslant 2$. Of the remaining fraction $(1 - f_0)$, the probability that a carbon atom is adjacent to an intercalate site is f_1 where $f_1 = 1$ for $C_{6n}X$ ($n \geqslant 2$), $f_1 = 3/4$ for $C_{8n}X$ ($n \geqslant 2$), $f_1 = 2/3$ for $C_{9n}X$ ($n \geqslant 2$), and $f_1 = 1/2$ for $C_{12n}X$ ($n \geqslant 2$). Thus, for $n \geqslant 2$, three distinct modes near the E_{2g_2} modes for pristine graphite are possible, and are denoted here as $E^{\circ}_{2g_2}$, E'_{2g_2} and E''_{2g_2}. In accordance with these geometrical considerations, the intensity of these modes will depend on the probabilities f_0 and f_1 according to $I(E^{\circ}_{2g_2}) \sim f_0\sigma^0/2$, $I(E'_{2g_2}) \sim (1 - f_0) \times (1 - f_1)\sigma'$ and $I(E''_{2g_2}) \sim (1 - f_0)f_1\sigma''$, the factor of 1/2 being inserted for the type 1 carbon atoms since the single plane E_{2g} mode contributes equally to the E_{2g_2} Raman-active and the E_{1u} infrared active modes when the AB planar stacking is present. The Raman scattering intensity is expected to exhibit a small dependence on intercalate species because the scattering intensity also depends on the Raman scattering cross section indicated here in terms of σ^0, σ', and θ''. The cross section can exhibit resonant enhancement effects due, for example, to resonance with the electronic levels of the intercalates. Study of the dependence of the scattering intensity on intercalate species and concentra-

TABLE 2

Vibrational modes* in graphite and C_xX**

C_2	Carbon atom planar mode frequencies (in cm^{-1})						Intercalate mode frequencies (in cm^{-1})	
	$\Gamma(E_{2g_2}) = 1582$			$M_{1g} = (560)^{\dagger\dagger}$ $M_{3g} = (1440)^{\dagger\dagger}$				
	$E^{\circ}_{2g_2}$	E'_{2g_2}	E''_{2g_2}	$E_{2g}(M_{1g})$	$A_{1g}(M_{1g})$	$E_{2g}(M_{3g})$	Solid X or free X molecules***	C_xX
C_xK		1599 [2]	$(1600)^{\dagger\dagger}$	563 [1]	562 [1]	1547 [1]	$63(\theta_D)$ $93(K_2)$	
C_xRb	1579 [3]	1602 [2] 1603 [3]	$(1602)^{\dagger\dagger}$ $(1603)^{\dagger\dagger}$	581 [1]	572 [1]	1480 [1]	$39(\theta_D)$ $57(Rb_2)$	
C_xCs	1579 [3]	1598 [2] 1604 [3]	$(1598)^{\dagger\dagger}$ $(1604)^{\dagger\dagger}$	596 [1]	579 [1]	1519 [1]	$26(\theta_D)$ $42(Cs_2)$	$33^{\dagger\dagger\dagger}$ [1] $24^{\dagger\dagger\dagger}$ [2, 3]
C_xBr_2	1583 [9] 1590 [2]	1603 [9] 1611 [2]	$(1617)^{\dagger\dagger}$				323(g) 300(s)	242 [22] 152 [22] 104 [22]
C_xIBr	1583 [4]	1603 [4]	$(1609)^{\dagger\dagger}$				268(g)	230 [21] 200 [21] 110 [21] 96 [21]
C_xICl	1586 [1]	1609 [1]	$(1638)^{\dagger\dagger}$				384(g)	186 [1] 103 [7] 98 [13]
C_xAsF_5			1635 [1] 1622 [2]				$733^{\dagger}$ (l)	$(612)^{\dagger\dagger}$ [1] $(640)^{\dagger\dagger}$ [2]

*The mode frequencies (cm^{-1}) are taken from Raman scattering data except as otherwise noted (see refs. 13 - 16).

**The intercalate (X) concentration $[1/(x + 1)]$ is indicated in the Table by the stage number, n, which is written in brackets as $[n]$.

***The stretching modes for the free diatomic molecules are from ref. 21. The entries marked (θ_D) are the Debye temperatures for the metals. The notation (g, l, or s) indicates gas, liquid, or solid.

†See ref. 19.

††Estimated as indicated in the text.

†††Heat capacity data of ref. 20.

tion could therefore provide information on the electronic structure of graphite intercalation compounds.

Experimentally, many graphite intercalation compounds exhibit only two types of E_{2g_2} Raman lines, one having $E^{\circ}_{2g_2}$-type characteristics and the other being a superposition of unresolved E'_{2g_2} and E''_{2g_2}-type modes. This behavior occurs when the intercalate modes which interact with the E'_{2g_2} modes are of very low frequencies, as in the alkali metals. This behavior can also be accounted for by assuming that the intercalate is free to hop from one equivalent site to another. For cases where the E'_{2g_2} and E''_{2g_2} modes are unresolved, then the intensity ratio for stage $n \geqslant 2$ becomes $I(E^{\circ}_{2g_2})/[I(E'_{2g_2}) + I(E''_{2g_2})] \sim [f_0/2](1 - f_0)[\sigma^0/\bar{\sigma}]$ where $\bar{\sigma}$ is an average of the cross sections σ' and σ'' for the E'_{2g_2} and E''_{2g_2} modes. Nemanich *et al.* [14] have successfully interpreted their spectra in the alkali metal compounds by not distinguishing between the E'_{2g_2} and E''_{2g_2} modes. However, for the low stage graphite–ICl compounds, we have resolved structures which we have associated with distinct E'_{2g_2} and E''_{2g_2} modes. Furthermore, some variation with intercalate species is also found for the dependence on intercalate concentration of the *intensity* of the upshifted mode for dilute halogen compounds. We interpret the reported results on the relative intensities of

the doublet components [13] of the Br_2 and ICl compounds to indicate a greater coupling between the carbon atoms to the ICl intercalate than to Br_2. This could arise if the ICl molecules are partly tipped out of the intercalate layer plane and the Br_2 lie in the plane, thereby giving rise to different Raman cross sections for the two intercalate species.

The perturbation of the graphite lattice modes produced by the intercalate is much greater for stage 1 compounds than for the higher stage compounds because in this case each graphite layer is fully surrounded by intercalate layers. Consequently, qualitatively different Raman spectra are observed for stage 1 compounds. Geometrical considerations, as discussed above, give $f_0 = 0$ and $f_1 = 1$ for the C_8X structure, every C atom lying adjacent to an intercalate on a neighboring layer plane. These geometrical differences are consistent with the major differences in the Raman spectra that are observed for stage 1 and higher stage compounds. Since the coupling to the intercalate planes is stronger for stage 1 compounds, a much larger variation with intercalate species is found in the Raman spectra for stage 1 compounds. For example, in the case of first stage C_8AsF_5, the Raman spectrum consists of a single, sharp, intense line, having a half-width of ~ 7 cm^{-1} and upshifted to 1 636 cm^{-1} [16]. This upshift is much greater than prevails for the higher stage AsF_5 compounds or for the variety of other higher stage compounds ($n \geqslant 2$) shown in Table 2. For the higher stage compounds a small monotonic increase in the frequency of the E'_{2g_2} lines occurs with increasing intercalate concentration until a stage 2 compound is reached. However, this frequency increase is small, much smaller than that observed in going from a stage 2 to a stage 1 compound.

By contrast, the Raman spectra for the alkali metal stage 1 compounds (see Fig. 8) are qualitatively different from spectra for the first stage C_8AsF_5 or for higher stage compounds. The spectra of Fig. 8 show a broad, asymmetric line at high frequencies and a sharp structure at lower frequencies. The peak of the broad line occurs at approximately the frequency of the zone edge M_{3g} mode shown in Fig. 3 and the peak of the sharp structure at ~ 560 cm^{-1} occurs near the frequency of the zone edge M_{1g} mode. Both the low- and high-frequency features are in this way associated with the in-plane folding of the Brillouin zone, which brings these M-point modes into the zone center. These results further suggest that the $E_{2g}(E_{2g_2})$ mode shown in Fig. 5(a) is highly perturbed in the stage 1 alkali metal compounds. Our failure to observe the $E_{2g}(E_{2g_2})$ mode in stage 1 alkali metal compounds (a mode which does appear in first stage C_8AsF_5) might be due to a large upshift and broadening of this line arising from crystalline imperfections.

The broad line around 1 500 cm^{-1} has the asymmetric Breit–Wigner lineshape [13, 15]. We attribute the large linewidth to mode coupling arising from both in-plane and c-axis zone folding effects. For the stage 1 compounds, there are no longer equivalent planar A and B carbon atom sites. Thus, the distinction between the E_{2g} and E_{1u} graphite modes is no longer relevant and zone folding effects for the M_{2u} and M_{4u} modes can also lead to

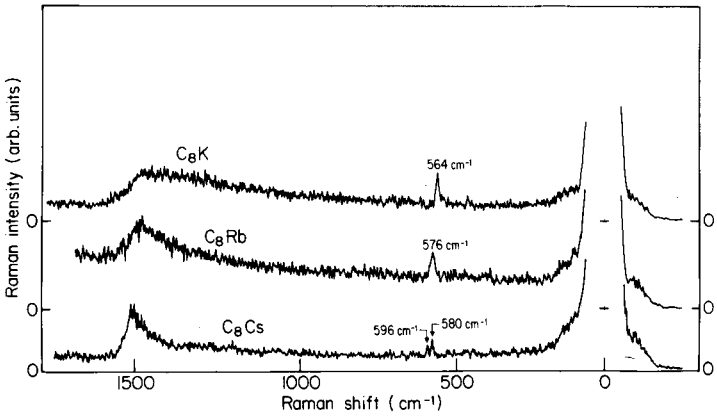

Fig. 8. Raman intensity for the stage 1 alkali metal compounds C_8K, C_8Rb and C_8Cs at 4 K over a wide frequency range using the Brewster angle back-scattering geometry.

Raman-active modes in the small Brillouin zone for the intercalation compounds. The c-axis folding arising, for example, from $\alpha, \beta, \gamma, \delta$ intercalate plane stacking gives rise to many more Raman-active $\vec{k} = 0$ modes in the small Brillouin zone. All zone center modes with the same symmetry will interact and become shifted in frequency. If the perturbation interactions are sufficiently strong and the crystal is imperfectly ordered, a large number of Raman-active modes spanning the frequencies of the upper optical modes in Fig. 3 can participate in the Raman process and a density of states model for unresolved or continuum modes results. The observation of a broad Breit–Wigner line for the stage 1 alkali metal compounds is indicative of a relatively strong interaction between the continuum modes and the graphitic M_{1g} and M_{3g} modes. A relatively strong interaction between the intercalate and graphite planes is consistent with results of Knight shift [17] and Mössbauer [18] studies, showing a large charge transfer between the alkali metal and graphite layers. We attribute the qualitative difference observed in Raman spectra for stage 1 alkali metal compounds and first stage C_8AsF_5 to a difference in the magnitude of the coupling between the intercalate and graphite layer planes and to the high frequency of the molecular AsF_5 breathing mode at 733 cm^{-1} [19].

Referring to the spectra for the stage 1 alkali metal compounds shown in Fig. 8, a second spectral feature appears in the vicinity of 560 cm^{-1} for C_8K, C_8Rb and C_8Cs. This spectral feature is shown in more detail in Fig. 9 using a polarization analysis to provide information on the symmetry properties of this structure. This symmetry analysis shows this structure to consist of two components, consistent with the identification of the lower frequency component with A_{1g} symmetry and the upper frequency component with E_{2g} symmetry. These symmetry assignments arise from the folding of the 3 equivalent zone edge M_{1g} modes into the Γ point of the smaller C_8X zone (see Fig. 2). This interpretation of the structure in the vicinity of 560 cm^{-1} provides the strong evidence for approximate D_{6h} symmetry and the application of zone folding concepts to the stage 1 alkali metal compounds. The peak frequencies for the two components of the structure are

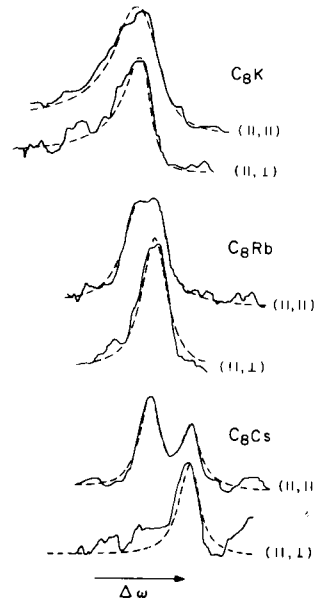

Fig. 9. Raman intensity at 77 K for stage 1 alkali metal compounds C_8K, C_8Rb and C_8Cs in the region of the M_{1g} mode for pristine graphite (560 cm^{-1}). The polarization effects (||, ||) and (||, ⊥) are consistent with the identification of the upper frequency component with E_{2g} symmetry and the lower component with A_{1g} symmetry. The dashed curves are a fit to the data using a Lorentzian line shape model.

given in Table 2 for each trace in Fig. 9. The largest splitting is observed in C_8Cs and, hence, the clearest symmetry assignment can be made in this case. For C_8Cs the doublet is observed in (||, ||) polarization (where both A_{1g} and E_{2g} are symmetry-allowed), but only a single line occurs for the (||, ⊥) polarization (where only E_{2g} is symmetry-allowed). The doublet is up-shifted in frequency by $\delta\omega$ and is split by a frequency $\Delta\omega$. If the ratio $(\Delta\omega/\delta\omega)$ is assumed to be independent of alkali metal species, then the splitting, $\Delta\omega$, follows the sequence $\{\sim 1, 9, 17\}$ for the {K, Rb, and Cs} compounds, respectively, and places the pristine graphite M_{1g} level at 560 cm^{-1}; we thus refer to this doublet structure as the 560 cm^{-1} structure. This identification of the doublet structure requires the M_{1g} level to lie lower than indicated in Fig. 3. However, such a lowering is also inferred by the low frequency recently reported for the A_{2u} infrared-active mode [6]. We attribute both the frequency shift, $\delta\omega$, and the frequency splitting, $\Delta\omega$, to an interaction of the zone-folded M_{1g} modes with coupled soft zone-center alkali-metal intercalate modes. This interpretation accounts for the frequency

upshift of the modes shown in Fig. 9 and for their dependence on intercalate species. Because of the much larger lattice constant of metallic Cs relative to that for Cs in C_8Cs and the more similar lattice constants for metallic K and Rb in comparison with C_8K and C_8Rb, respectively, a larger lattice distortion is expected for C_8Cs than for C_8K and C_8Rb.

No Raman spectra for the intercalate species have been observed in the alkali-metal compounds. We estimate the frequency of these intercalate modes to be low and comparable with $k\theta_D$ where θ_D is the Debye temperature. For the alkali metals, $k\theta_D$ is approximately 63 cm^{-1}, 39 cm^{-1}, and 26 cm^{-1} for metallic K, Rb, and Cs, respectively. Some evidence for a soft intercalate mode is provided by a low-temperature anomaly at 33 cm^{-1} observed in the heat capacity of C_8Cs [20].

By contrast to these very low frequency modes, the halogen intercalates exhibit modes at intermediate frequencies associated with molecular stretching modes. Evidence in support of the identification of these modes with the intercalate species comes from: (1) the strong dependence of the frequencies and characteristics of these modes on intercalate species; (2) the proximity of the observed modes to the stretching modes for the corresponding free molecules. In the free molecules these modes are at $\omega(X_2^\circ) = 323$ cm^{-1}, 268 cm^{-1}, and 384 cm^{-1} for molecular Br_2, IBr and ICl, respectively [21]. The Raman spectrum associated with these modes in graphite–Br_2 is down-shifted in frequency to $\omega(X_2) = 242$ cm^{-1} because of a coupling of this intercalate mode to the E'_{2g_2} mode for carbon atoms in the adjacent plane. This interaction causes the graphitic mode to be upshifted in frequency and the intercalate mode to be downshifted in frequency by approximately equal amounts: $\omega^2(E''_{2g_2}) - \omega^2(E'_{2g_2}) \cong [\omega^2(X_2^\circ) - \omega^2(X_2)]$. This relation has been used in Table 2 to estimate the position of the E''_{2g_2} modes for the various halogen compounds. There are a variety of reasons why this formula may not be quantitatively correct for the halogen compounds. For these compounds the unit cell is large and differs from the C_8X structure discussed here. Also, the amount of charge transfer to the plane adjacent to the intercalate layer is smaller than for the alkali metals.

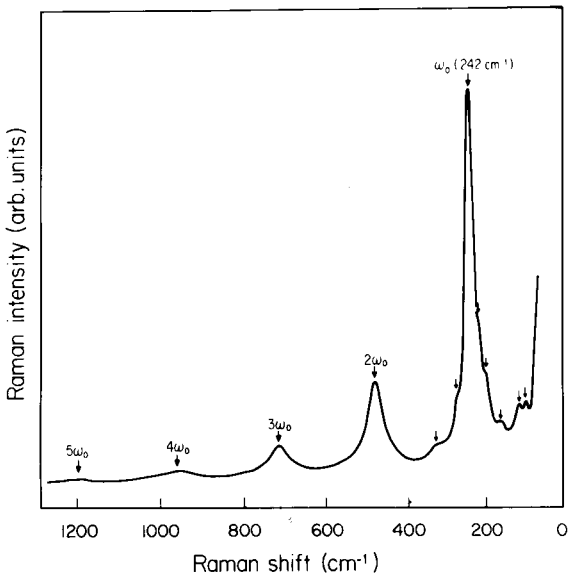

Fig. 10. Raman intensity in the region of the Br_2 stretching mode at 77 K using the Brewster angle backscattering geometry for a 2.7 mole% Br_2 graphite–Br_2 compound. The structure identified with the Br_2 stretching mode in the intercalation compound is indicated by ω_0 and harmonics of this structure are indicated. Additional weak structures are indicated by arrows.

The most striking feature of the spectrum in Fig. 10 is the strong harmonic structure of $\omega(Br_2) = 242$ cm^{-1}. We attribute these harmonics to a resonant Raman process associated with the Br_2 electronic levels. In addition, Fig. 10 shows additional fine structure indicated by arrows. This fine structure may be due to the presence of small numbers of ionized intercalate species which are assumed to order at low temperatures, since this fine structure is well resolved at 77 K but not at room temperature. These ordering effects have not yet been studied in detail [13]. Polarization studies of these intercalate modes are expected to yield valuable information on molecular alignment effects and on the associated order–disorder phenomenon. Raman lines associated with the molecular intercalate AsF_5 are predicted by the above formula and are listed in Table 2 in parentheses.

In the above discussion, emphasis was given to the modifications to the Raman spectrum of pristine graphite caused by intercalation and how these modifications could be explained in terms of a perturbation to the

graphite lattice mode structure. Correspondingly, intercalation produces changes in the infrared spectrum of pristine graphite. In this connection, a preliminary account of infrared spectra in graphite–Br_2 and graphite–ICl has recently been reported [5]. Infrared spectra on these materials in the lattice mode region are complicated by free carrier and electronic interband effects. For example, for pristine graphite (and also for intercalation compounds with low intercalate concentrations) the lattice mode structure appears as a peak in the reflectivity, whereas in the more highly conducting low stage compounds, the lattice mode structure appears with a very different line shape, exhibiting a reflectivity minimum. To extract lattice mode frequencies from these spectra, a fit must be made to the observed reflectivity line shape where the background contributions to the dielectric constant from free carriers and electronic transitions are included. Such an analysis of the observed infrared spectra reveals a single E_{1u} infrared-active line at 1 588 cm^{-1} in pristine graphite [1, 5, 6]. A mode at this frequency is also found in the various intercalation compounds studied to date [5], but the intensity of this mode decreases with increasing intercalate concentration. In addition, another mode at ~1 582 cm^{-1} (at the $E^{\circ}_{2g_2}$ mode frequency) is found in the intercalation compounds and the intensity of this mode increases with increasing intercalate concentration. Although only scanty experimental infrared data are presently available, infrared spectroscopy of lattice modes in graphite intercalation compounds appears to be a complementary technique to Raman spectroscopy for studying the nature of the coupling between the carbon atoms and the intercalate species in these materials.

REFERENCES

1 L. J. Brillson, E. Burstein, A. A. Maradudin and T. Stark, in D. L. Carter and R. T. Bate (eds.), Proc. Int. Conf. Phys. Semimetals and Narrow Gap Semiconductors, Dallas, Texas, 1970, Pergamon Press, New York, 1971, p. 187.
2 L. J. Brillson, Ph. D. Thesis, Dept. of Physics, Univ. Pennsylvania, Philadelphia, PA., U. S. A., 1972, unpublished data.
3 F. Tuinstra and J. L. Koenig, J. Chem. Phys., 53 (1970) 1126.
4 R. A. Friedel and G. C. Carlson, J. Phys. C., 75 (1971) 1149.
5 L. E. Schmutz, D. D. L. Chung, R. A. Wachnik, P. C. Eklund and M. S. Dresselhaus, Bull. Am. Phys. Soc., 22 (1977) 420.
6 R. G. Nemanich, S. A. Solin and G. Lucovsky, Mater. Sci. Eng., 31 (1977) 157.
7 R. Nicklow, N. Wakabayashi and H. G. Smith, Phys. Rev. B, 5 (1972) 4951.
8 G. Lucovsky and R. Zallen, personal communication.
9 G. Dresselhaus and M. S. Dresselhaus, to be published.
10 W. Rüdorff and E. Schulze, Z. Anorg. Allg. Chem., 277 (1954) 156.
11 G. S. Parry, Mater. Sci. Eng., 31 (1977) 99.
12 D. D. L. Chung, G. Dresselhaus and M. S. Dresselhaus, Mater. Sci. Eng., 31 (1977) 107.
13 J. J. Song, D. D. L. Chung, P. C. Eklund and M. S. Dresselhaus, Solid State Commun., 20 (1976) 1111.
14 R. G. Nemanich, S. A. Solin and D. Guérard, Phys. Rev. B 16, to be published.
15 P. C. Eklund, G. Dresselhaus, M. S. Dresselhaus and J. E. Fischer, Phys. Rev. B 16, to be published.
16 P. C. Eklund and E. R. Falardeau, unpublished data.
17 G. P. Carver, Phys. Rev. B, 2 (1970) 2284.
18 L. E. Campbell, G. L. Montet and G. J. Perlow, Phys. Rev. B, 15 (1977) 3318.
19 L. C. Hoskins and R. C. Lord, J. Chem. Phys., 46 (1967) 2402.
20 U. Mizutani, T. Kondow and T. B. Massalski, Phys. Rev. B 16, to be published.
21 G. Herzberg, Spectra of Diatomic Molecules. Van Nostrand, Princeton, N. J., 1945.